

Design of MEMS based three-axis motion stage by incorporating a nested structure

Y-S Kim^{1,2}, N G Dagalakis² and S K Gupta¹

¹ Department of Mechanical Engineering and Institute for Systems Research, University of Maryland, College Park, MD 20742, USA

² Intelligent System Division, Engineering Laboratory, National Institute of Standards and Technology, Gaithersburg, MD 20899, USA

E-mail: mk37do@gmail.com

Received 4 January 2014, revised 6 May 2014

Accepted for publication 8 May 2014

Published 5 June 2014

Abstract

A new design of three degrees-of-freedom (DOF) translational motion stage (XYZ stage) is presented in this paper. This XYZ stage is based on MEMS and designed by combining three existing one-DOF motion stages through a nested structure. By utilizing the previously developed stages, this approach can reduce the effort for the design and analysis steps and ensure reasonable reliability. For successful implementation, electrical connection to the engaged stages, electrical isolation among them, and additional floating frames are introduced for the chosen one-DOF motion stages. With these features, the presented XYZ stage is successfully fabricated and demonstrates the range of motion of 53.98, 49.15, and 22.91 μm along X, Y, and Z axes, respectively. The coupled motion errors among the engaged stages can be reduced to be less than 1 μm with the proposed compensation method.

Keywords: MEMS, three-axis, motion stage, nested structure, serial kinematic mechanism

(Some figures may appear in colour only in the online journal)

1. Introduction

Micro-scale devices based on MEMS have various advantages, such as their small form factors, low cost from batch process, and nano-meter level resolution [1–4]^{3,4}. These strengths have made MEMS-based systems attractive in various applications, such as micro-assembly [1], manipulation [2], and metrology [3]. However, many MEMS fabrication methods can only realize planar designs and hence have limited operations. Multiple degrees-of-freedom (DOF) motion or a combination of in-plane motions and an out-of-plane motion are still difficult to implement or require considerable efforts in their design process and fabrication process [2, 4]. In contrast to MEMS motion stages, the typical approach used in conventional meso-scale motion stages is to stack up multiple stages to generate various motions^{3,4}. In this case, existing designs or stages can be reused, which can not only save the total

design process time, but also provide predictable reliability. However, this method is difficult to utilize with MEMS; the manual stacking-up operation can damage MEMS devices or provide relatively poor accuracy and huge errors. Moreover, the electric connection to the devices which are stacked on others is also challenging. Due to these reasons, it is rare to find MEMS-based motion stages utilizing stacking-up or embedding approaches.

Many MEMS motion stages have been developed for two or three DOF motion, especially for the combination of in-plane translational and in-plane rotational motions [5–7], but MEMS stages for three-axis motion or XYZ motion are not common [8–10]. The main reason for this is that the difference in design and fabrication between the out-of-plane motion (called a Z-motion) and the in-plane motions (called an X-motion or a Y-motion) is too large to combine them together. In order to overcome this issue, additional efforts and fabrication methods have been tried; the focused ion beam (FIB) milling for the out-of-plane slope [8], wafer bonding for parallel plate type electrostatic actuation [9], or silicon-on-insulator (SOI) wafer for a dual layer [10] were used for the

³ *Low Inertia 6DOF Parallel Kinematic Mechanisms (PKM) from Physik Instrumente* www.physikinstrumente.de/news/pdf/Hexapod_fold_finCp.pdf

⁴ *Pizeo-University Parallel and Serial Kinematics/Metrology* www.physikinstrumente.com/en/products/prdetail.php?sortnr=400800.20

Table 1. 3 DOF MEMS-based positioning stages.

Reference	Range of motion						Features
	X-axis		Y-axis		Z-axis		
	Motion (μm)	Voltage (V)	Motion (μm)	Voltage (V)	Motion (μm)	Voltage (V)	
[8]	1.1	100	1.1	100	1.1	100	FIB milling
[9]	25	30	25	30	3.5	14.8	Wafer bonding
[10]	19	100	19	55	2.12	200	SOI wafer

Z-motions. With these approaches, researchers have achieved various ranges of motion, as listed in table 1. These results indicate that the resulting Z-motions are considerably smaller than X- or Y-motions and relatively high driving voltages are needed to realize them. This smaller Z-motion comes from the structural difference between in-plane structures and out-of-plane structure in MEMS fabrication methods. The high driving voltages are not compatible with common electric circuits and attracting dust easily results in electrical shorting of circuits. Based on the limitations in MEMS three-axis motion stages, it is beneficial to develop a three-axis motion stage having larger displacements than existing designs with less effort and time in development.

In this paper, the design, fabrication, and test of a MEMS-based three-axis or three-DOF positioning stage (called an XYZ stage) is presented by utilizing a nested structure. The nested structure is the integration method through nesting a chosen Z stage into a selected Y stage which is also embedded into an X stage. In order to implement this approach efficiently, two one-DOF stages are carefully selected from existing stages; two in-plane motion stages for the X stage and the Y stage and one out-of-plane motion stage for the Z stage. The chosen X stage consists of a bent-beam type electrothermal actuator and a moving plate and the Y stage is identical to the X stage, but its orientation is orthogonal to the X stage. The moving plates are utilized to embed an independent device for the nested structure. In this case, the nested structure can be implemented by embedding the full Z stage into the moving plate of the Y stage and embedding this Y stage onto the moving plate of the X stage. The Z stage is based on the buckling effect [11], which generates larger displacement than bi-morph type actuators [12, 13] with the same foot prints. All three motion stages are chosen for their fabrication processes compatibility to each other. The integration strategy for the nested structure, basic principles, numerical analyses for the chosen stages and actuator, and the experimental results are discussed in the following sections. For the successful operations of the XYZ stage, additional supporting frames, blocks and embedded electric paths are also introduced and described in detail in this paper.

2. Design of the three-DOF motion stage

The presented XYZ stage is designed to generate translational motions along the X, Y, and Z axes. For the three-DOF translational motions, at least three independent single DOF

actuators or actuating mechanisms are required. Since this study focuses on utilizing existing designs, appropriate in-plane and out-of-plane one-DOF motion stages are selected from previous designs. The conceptual designs of the chosen systems are shown in figure 1; figure 1(a) for the X stage, figure 1(b) for the Y stage, and figure 1(c) for the Z stage. The X and Y stages are composed of one bent-beam type electrothermal actuator, four links, and one moving plate [14–16]. Two of four flexure links for each of the X and Y axes stages are used as a lever for large stroke. The actuator actuates the levers which amplify the displacement of the moving plate. The fabrication of the X stage and the Y stage is based on the SOI multi-user multi-processes (SOI-MUMPs) for SOI wafers [17] and generates the force of more than 45 mN and the displacement of $50\mu\text{m}$ [16]. The Z stage is also chosen from existing designs [18, 19] and generates $25\mu\text{m}$ [18] to $80\mu\text{m}$ [19] displacements depending on the designs reported in the papers.

The integration strategy for the three independent stages described above is schematically shown in figure 1 [20]. The moving plate of the X stage is utilized to embed the Y stage, which is also designed to contain the Z stage as shown in figures 1(a), (b) and (c). The expected merged shape is shown in figure 1(d). This approach is called the nested structure, through which the XYZ stage can be built. Both ends of the bent-beam type electrothermal actuators in the XYZ stage should keep a same gap during their operations for efficient performance. To meet this requirement, a floating frame is introduced. This floating frame is attached to the bottom of the actuator and stiff enough to hold both ends of the actuator in their position firmly. This frame also should be free to move in order not to prevent any motion generated by the XYZ stage. For this purpose, a dual layer approach is utilized through SOI wafers in this study; SOI wafers are bi- or triple-layer structures. If the XYZ stage is built on the top layer of the SOI wafers and the floating frame is made of the bottom layer of the SOI wafers, then additional bonding process can be avoided, since the two layers are already attached to each other.

The X stage, the Z stage, and additional features like the floating frames are explained in the following section separately. Since the Y stage is identical to the X stage, the X stage only is discussed. These explanations include working principles, basic analysis, and finite elements analysis (FEA) results. There is no modification or significant change made in the chosen X stage [16] except the moving plate size and the floating frame; the moving plate is adjusted to embed the other device without any lack of space. The Z stage is composed of one shaft and the actuator used for the Z-motion stage [18].

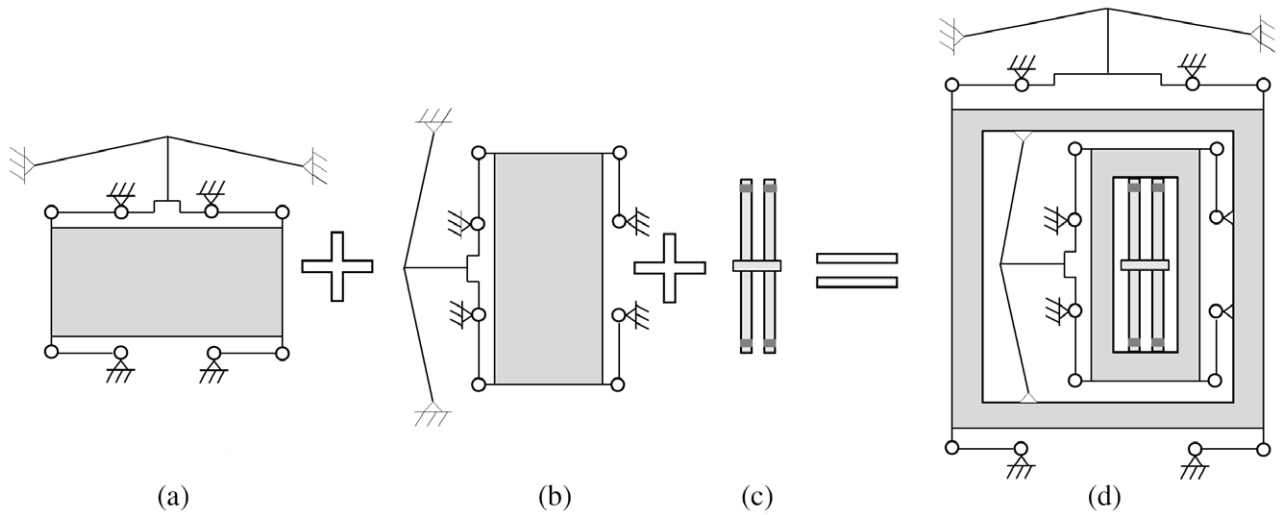


Figure 1. The integration strategy for the XYZ stage: (a) the X stage; (b) the Y stage; (c) the Z stage; (d) the integration of (a), (b) and (c) for the XYZ stage.

2.1. The X stage and the Y stage

The X stage is composed of a bent-beam type electrothermal actuator, one moving plate, and four links [14]. The schematic diagram of the X stage is shown in figure 2, where the arrows stand for the expected direction of motion, the circles represent rotational flexure hinges as compliant mechanisms, and the solid lines for rigid links. The four links support the four corners of the moving plate, so the moving plate can be fully constrained. The two of the four links work as a lever which transfers the displacement to the moving plate with the amplifying ratio of 1:10. Due to this lever, the motion direction of the moving plate is opposite to that of the actuator. The details about the X stage are described in the previous study [15].

In the X stage, the combination of the moving plate and the actuator can be regarded as the combination of springs in a parallel configuration. In this case, the expected displacement of the moving plate can be expressed [16] as:

$$U_{\text{plate}} = \frac{F_{\text{actuator}}}{K_{\text{actuator}} + K_{\text{plate}}}, \tag{1}$$

where the subscript ‘plate’ indicates the moving plate and the subscript ‘actuator’ means the electrothermal actuator. The term U stands for displacement, F for force, and K for stiffness. Each term in equation (1) can be expanded as:

$$F_{\text{actuator}} = 2ab\Delta T_{\text{ave}}EWT \sin \theta \tag{2}$$

$$K_{\text{actuator}} = 2 \left(\sin^2 \theta + \cos^2 \theta \frac{12I}{WTL^2} \right) \frac{EWT}{L} \tag{3}$$

$$K_{\text{plate}} = \frac{n^2 m}{L^2 C_z} \tag{4}$$

where, C_z is the compliance of the rotational flexure hinge, n is a lever ratio, and m is the number of the links. The details and dimensions for other terms are explained in table 2.

The temperature rise is the average temperature rise from the room temperature of 20 °C and is the maximum

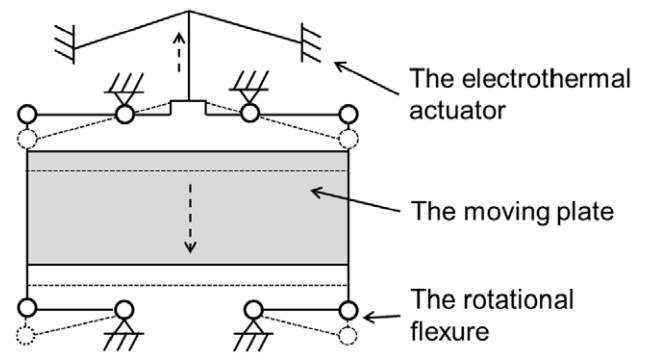


Figure 2. The schematic diagram of the X stage.

temperature rise in the actuator. In this case, temperature rise can be expressed based on the material properties of silicon [23] as:

$$\Delta T_{\text{ave}} = \frac{V^2}{3k\rho} = \frac{2}{3} \Delta T_{\text{max}} \tag{5}$$

where V is a voltage applied to the actuator, k is the thermal conductivity of silicon, and ρ is the resistivity of silicon. Their material properties are cited from the previous research [16]. Based on equations (2)–(5), equation (1) can be written as:

$$U_{\text{plate}} = \frac{2abEWT \sin \theta}{\left(\sin^2 \theta + \cos^2 \theta \frac{12I}{WTL^2} \right) \frac{EWT}{L} + \frac{n^2 m}{L^2 C_z}} \Delta T_{\text{ave}} \tag{6}$$

where each design parameter is explained with its dimension in table 2. From equation (6), the output displacement of the moving plate is expected to be a linear function of the average temperature rise in the actuator. With equation (5), equation (6) can be expressed as:

$$U_{\text{plate}} = \frac{2abEWT \sin \theta}{3k\rho \left(\sin^2 \theta + \cos^2 \theta \frac{12I}{WTL^2} \right) \frac{EWT}{L} + \frac{n^2 m}{L^2 C_z}} V^2 \tag{7}$$

Equation (7) shows that the displacement of the moving plate is also proportional to the square of the driving voltages, which

Table 2. Design parameters in the X stage, the Y stage and the Z stage.

Symbol	Design parameter	Values
W	Beam width	$23\ \mu\text{m}$
θ	Beam angle	3°
L	Beam length	$1000\ \mu\text{m}$
L_l	Link length	$1000\ \mu\text{m}$
T	Beam thickness	$30\ \mu\text{m}$
b	Number of beams	15
α	Coefficient of thermal expansion	2×10^{-6}
C_z	The compliance of the rotational flexure hinges	$7.52\ \text{Nm}\ \mu\text{rad}^{-1}$
E	Young's modulus of silicon	169 GPa
k	Thermal conductivity	$50\ \mu\text{m}$
m	Lever ratio	10
I	Area moment of inertia	–
ρ	Resistivity of silicon	$2 \times 10^{-3}\ \Omega\ \text{cm}$
ΔT_{ave}	Actuator average temperature	–
ΔT_{max}	Actuator maximum temperature	$< 530^\circ\text{C}$
U_{plate}	Platform displacement	$45\text{--}60\ \mu\text{m}$
V	Driving voltage	$1\text{--}8.5\ \text{V}$
e	The notch depth for the Z stage	$7.5\ \mu\text{m}$
L_z	Beam length for the Z stage	$1000\ \mu\text{m}$
P, P'	Eccentric load in the Z stage	–
L_w	Beam width for the Z stage	$33\ \mu\text{m}$

is similar to the findings of previous electrothermal actuator studies [21, 24]. This property can be utilized to reduce the coupled motion errors in the experimental section to control the moving plate precisely.

The maximum displacement of the moving plate is determined by a structural failure or a maximum reliable temperature of silicon. Since the structural limit is well described in the previous study [16], the temperature limit only is discussed in this paper. Above the temperature limit, plastic deformation initiates in silicon. Various temperatures have been reported for this limit; 550°C [25], 600°C [26], or 900°C [27]. The lowest value among them is selected as the maximum temperature limit in this study for a reliable operation. The room temperature is measured as approximately 20°C and the maximum temperature change (ΔT_{max}) is set to be 530°C .

Based on the above temperature limit, the design parameters listed in table 2 and the material properties of silicon [16], the mechanical behavior of the X stage is calculated in FEA. For this FEA, the ends of the rotational flexure hinges and the bottom side of the moving plate are assumed to connect to a heat sink at room temperature for its thermal boundary condition. The maximum allowable temperature of 550°C is applied to the actuator as an external thermal excitation to calculate its displacement. The corresponding mechanical behavior of the X stage is shown in figure 3(a) generating the displacement of $62.7\ \mu\text{m}$ larger than the maximum displacement of the X stage. When the X stage is stable under this large displacement, the stage will be reliable within its maximum displacement. The calculated stress, in particular the von Mises stress, is almost zero over most of the area of the stage except for the rotational flexure hinges, which have a stress of 1.47 GPa. This stress distribution pattern indicates that most of the deformation occurs in the rotational flexure hinges and plastic deformation is hardly expected with the yield strength of 6–7 GPa. This result fits well with the response of the X stage, though not the Y stage, because the Y stage is located inside the moving plate of the X stage and has different thermal and structural boundary conditions.

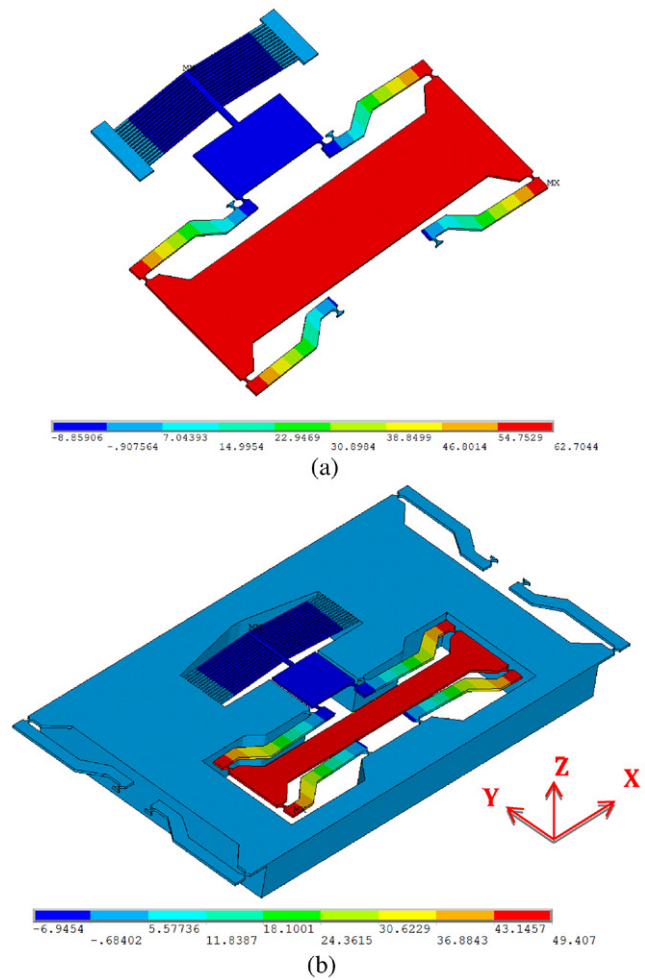


Figure 3. Mechanical response to FEA with actuator temperature rise of 530°C : (a) the X stage with a displacement of $62.7\ \mu\text{m}$ (unit in μm); (b) the Y stage with a displacement of $49.4\ \mu\text{m}$ (unit in μm).

The expected mechanical behavior of the Y stage is shown in figure 3(b). This FEA is also based on the same test condition applied to the X stage. The calculated maximum

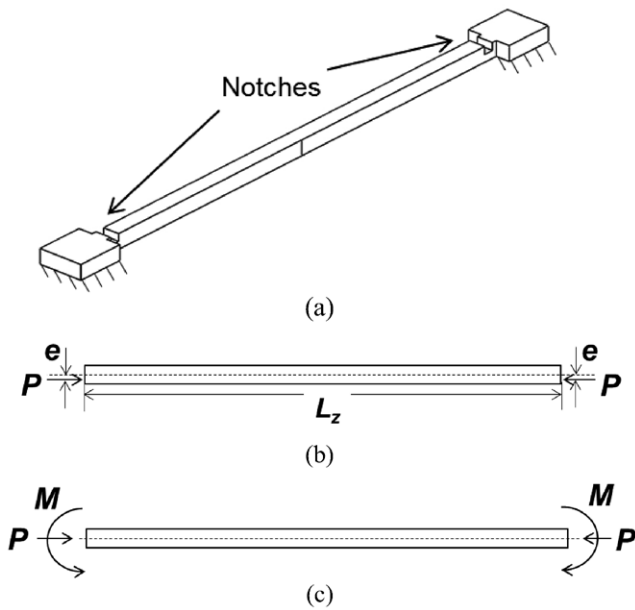


Figure 4. The design of the Z stage; (a) the side view; (b) a free-body diagram of (a); (c) the converted free-body diagram of (b) (L_z : beam length, P : repulsive force, M : a bending moment, e : eccentric distance from the central line).

displacement of the Y stage is $49.1 \mu\text{m}$, which is smaller than the X stage. This FEA shows that this difference comes from the structural boundary conditions; the bent-beam type electrothermal actuator and the pivots in the lever require firmly fixed anchors at its ends for efficient operation. However, the Y stage is supported by the floating frames to avoid any interference with the motion of the X stage. This floating frame is the thick block underneath the Y stage, which is not a perfect rigid body and not capable of holding the pivots in their position without any minor deformation. In this case, some amount of force generated by the electrothermal actuator will be used to deform the floating frame. Thus this difference results in a shorter stroke than the X stage as simulated using FEA.

2.2. The Z stage

The Z stage is selected from out-of-plane electrothermal actuators [18, 19], which is made up of four flat beams and one shaft rod. Each beam consists of one flat beam and two notches as shown in figure 4(a). The two notches are located near both ends of the beam and lead to a pop-up motion in the Z stage. When the electric current flows through the beam, Joule heating causes thermal expansion of the beams. This thermal expansion can be regarded as a repulsive force P from both its ends. The line the repulsive force P is applied has a distance from the central line of the beam with e as indicated in figure 4(b). L_z in figure 4(b) is the total length of the beam and its dimension is in table 2. Due to the notches, this repulsive force P generates an eccentric load. This eccentric load P can be expressed as a combination of a beam center line load P and a bending moment M whose converted free-body diagram is shown in figure 4(c). This diagram indicates that the eccentric load bending moment can be utilized to generate the out-of-plane motion of the beam. In this case, the deformation profile

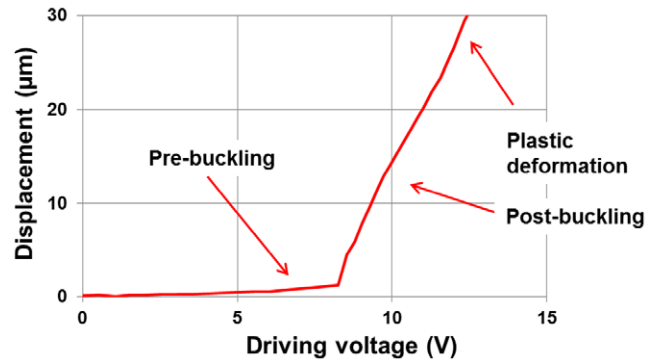


Figure 5. The mechanical behavior of the Z stage in an experiment.

at pre-buckling mode or pure thermal expansion mode can be expressed [28] based on a fixed-fixed boundary condition as:

$$y = e \left[\tan \left(L_z \sqrt{\frac{P}{EI}} \right) \sin \left(\sqrt{\frac{P}{EI}} x \right) + \cos \left(\sqrt{\frac{P}{EI}} x \right) - 1 \right] \quad (8)$$

where, I is the area moment of inertia of the beam and the other terms are listed in table 2. This thermal expansion by the bending moment M generates a smaller stroke than the X stage and this result makes the expected workspace look like a thin pizza box. Many commercially available XYZ stages have tried to provide a workspace close to a cubic-shape for more convenience⁵. In order to generate a more practical workspace in MEMS, the range of motion of the Z stage needs to be close to that of the X stage. For this purpose, the chosen Z stage utilizes a buckling [19]. The buckling is also called a wrinkling and commonly occurs in thin plate or long slender beams [28, 29]. Since the two notches already determine the deformation direction, this buckling accelerates this deformation without changing its direction.

The mechanical behavior of the Z stage is composed of three different modes as described in figure 5; the pre-buckling, the post-buckling, and the plastic deformation. The pre-buckling mode is the bending moment by pure thermal expansion of the beams at early stage. The thermal expansion of the beam is the main thrust to generate a few micro meter motions with low voltages. Above the critical voltage, the beam starts buckling and the post-buckling mode begins. In this mode, the out-of-plane displacement accelerates rapidly. This mode will be used in the XYZ stage to generate large displacement. Above the post-buckling mode, the plastic deformation mode starts, which damages the beams. The deformed beams are not able to return to their original positions and show different mechanical behaviors, so these beams cannot be utilized again. In order to prevent this plastic damage, the available driving voltage range should be carefully chosen within its elastic range.

The FEA is utilized to better understand the mechanical behavior of the Z stage. Figure 6 shows the expected structural response to the external excitation for the temperature of $550 \text{ }^\circ\text{C}$ in the actuator for pre-buckling mode. This result shows that the notches guide the Z stage well to generate a popping up motion. The moving plate of the Y stage does not show any structural deformation indicating that the floating frame in the moving plate performs its duty well. For stress

⁵ Physik Instruments P-611.3 NanoCube XYZ Piezo Stage www.physikinstrumente.com/en/products/prdetail.php?sortnr=201700

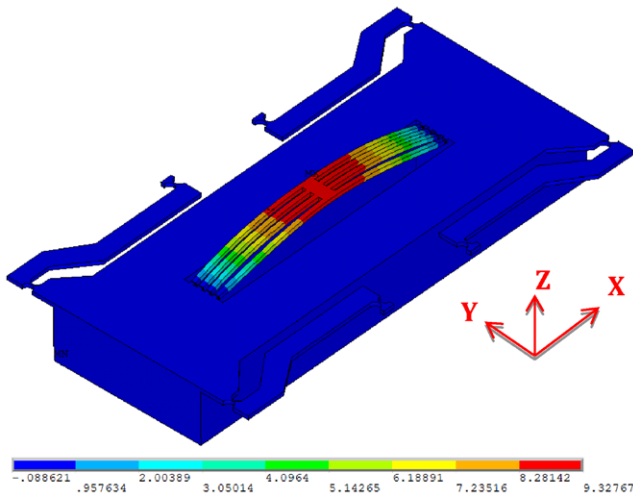


Figure 6. The mechanical response of the Z stage to the temperature rise of 530 °C as an external excitation.

distribution analysis an external excitation is applied to the actuator to generate an out-of-plane motion of $30\mu\text{m}$. For this displacement the von Mises stress distribution over the Z stage is calculated. This value is less than 1.5 GPa and its maximum occurs inside the notches. The expected maximum displacement of the Z stage is less than $22.91\mu\text{m}$, so this stress distribution implies that no structural failure is expected in the Z stage with the displacement of $22.91\mu\text{m}$.

3. Fabrication

The main fabrication process of the presented XYZ stage follows the SOI-MUMPs [17] and uses SOI wafers as a starting material. One more partial etching step was added to the SOIMUMPs for the fabrication of the notches in the Z stage. The SOI wafer selected for the XYZ stage is composed of a $30\mu\text{m}$ thick device layer, a $400\mu\text{m}$ thick handle layer, and a $2\mu\text{m}$ thick buried oxide layer. The main processes consist of one metal deposition step and three etching steps. The first step is the metal deposition of four layers for electrical connections; 100 nm of chrome, $2\mu\text{m}$ of copper, 100 nm of titanium, and $0.2\mu\text{m}$ of gold. This metal deposition is relatively thicker than conventional metallization for reliable electric connection, since the Z stage and the Y stage have longer electrical paths in the nested structure. The second step is to build the main device shown in figure 7(a) onto the device layer through deep reactive ion etching (DRIE). The third step is to etch the notches in the Z stage by partial DRIE. The fourth step is to etch the additional structures in the handle layer indicated by A, B, C, and D in figure 7(d). After a series of three etchings, the buried oxide layer is removed to release the Y stage and the Z stage. Details for each step are explained in SOI-MUMPs [17] and the cited studies [14–16, 18, 19].

Based on the fabrication processes described above, the XYZ stage can be successfully implemented. The frontal views of the fabricated main devices are shown in figure 7(b). This image was taken inside an SEM. In figure 7(b), the bright white color indicates the metal layer and the gray area silicon. In the middle of figure 7(b) is the Z stage. A zoom-in of this image provides a better view of the Z stage shown

in figure 7(e) where a probe is embedded on the middle of the Z stage for manipulation applications. A detailed view of the electric connection over the rotational flexure hinge is also shown in figure 7(f). As shown in figure 7(e), the Z stage is surrounded by the Y stage, which is also surrounded by the X stage shown in figure 7(b). These images show the cascaded pattern in the nested structure clearly.

For successful implementation of the nested structure, three features are added: the floating frames, the remote electric access, and electrical isolation among the X, Y, Z components of the system. The floating frames are built from the device layer or the bottom layer of a SOI wafer as indicated by A and B in figure 7(d). The floating frame A holds the Y stage in its position and supports both ends of the actuator in the Y stage and the floating frame B supports the Z stage for proper operation. Both frames are free to move along the X or Y axes to avoid any interference with the X or Y stages. This is because the electrothermal actuators used in the Y stage and the Z stage need anchors for their proper operation, which is contrary to electrostatic actuators.

Remote electrical access to the Y stage and the Z stage is also important and requires additional features. Conventional wire-bonding machines utilize a few mg level forces to bond the wires on the metal pads. This amount of force can damage the Y stage or the Z stage which are suspended from the X stage. In addition to this problem, the stiffness or the shape of the wire itself can distort the motion of the target stages [30]. In order to overcome these constraints, the deposited electric connection is adapted to connect the Y stage and the Z stage with the external electrical power source available for conventional wire-bonding. These electric paths are deposited on the device layer during the fabrication and shown in figures 7(a), (b), (e) and (f). This electric path is also connected over the rotational flexure hinge as shown in figure 7(f).

The electrical isolation among the stages is also necessary to reduce the coupled motion error from any electrical current leaks. For this electric isolation, trenches surround the electrothermal actuator as shown in figure 7(a) or figure 7(b). These trenches are physical gaps on the device layer and force the electric current to flow to the designated actuator only. The floating blocks C and D hold the trenches in the X stage and the Y stage, respectively. These floating supporting blocks are made of the handle layer in the SOI wafer, which skips additional processes like wafer bonding or multi-layer deposition and saves the total process time.

4. Experimental characterization of the MEMS three-axis stage

4.1. The range of motion

The maximum range of motion of the fabricated XYZ stage is experimentally measured. For the experimental settings, three DC power supplies (Agilent Model 3322A⁶) are connected to

⁶ Certain commercial equipment is identified in this paper to adequately describe the experimental procedure. Such identification does not imply recommendation or endorsement by the National Institute of Standards and Technology nor does it imply that the equipment identified is necessarily the best available for the purpose.

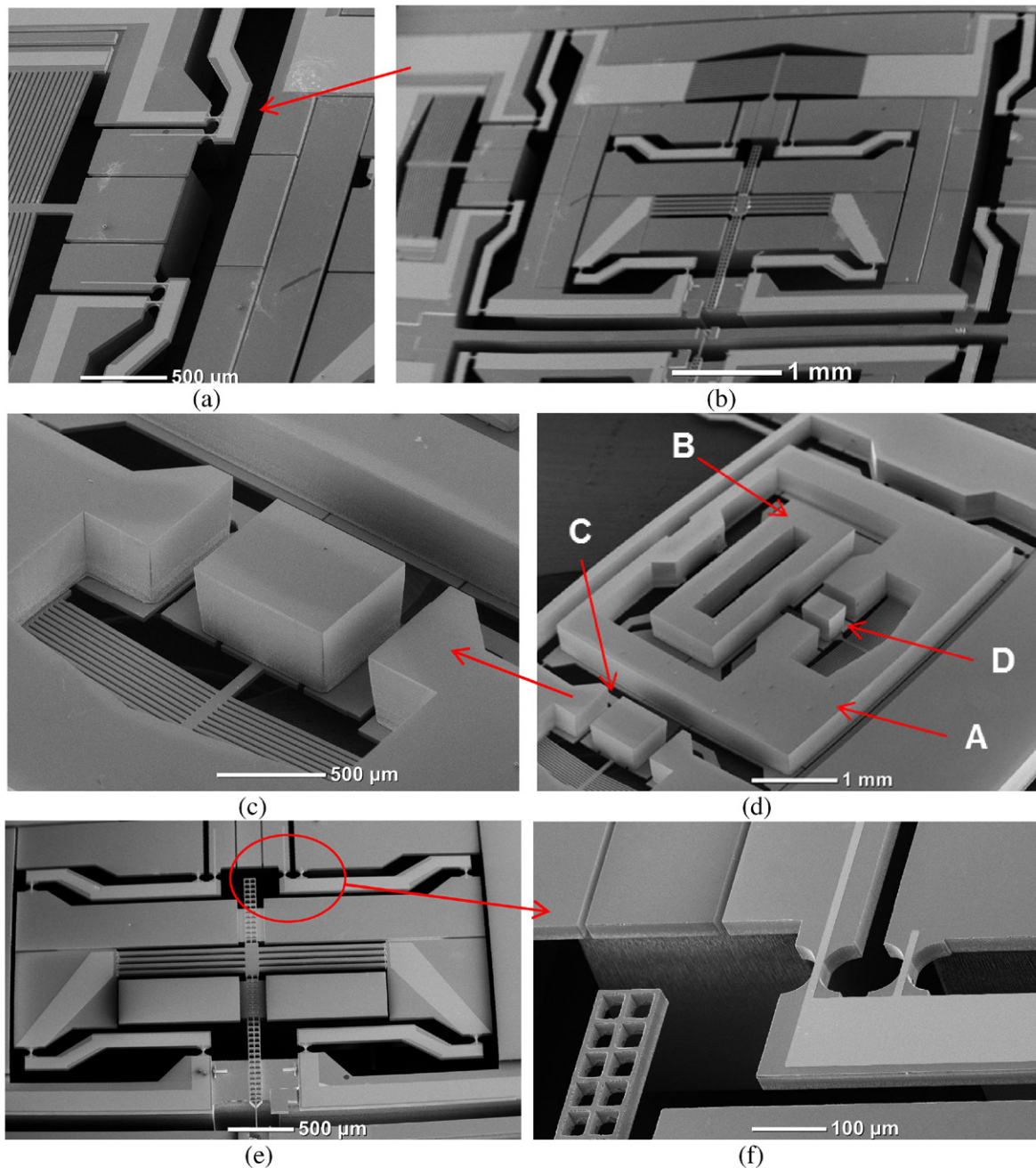


Figure 7. Fabricated XYZ stage: (a) close-up view of the actuator in the X stage; (b) frontal view of the XYZ stage; (c) floating block C in the backside of (a); (d) backside view of the XYZ stage for the floating frames and floating blocks; (e) zoom-in view of the Z stage and the moving plate of the Y stage; (f) deposited electrical connectivity wire paths over the flexure link (left) and the rotational flexure hinge (right).

the XYZ stage as an electric source. When the operator controls the three supplies, the corresponding behaviors from the XYZ stage are measured with an optical profiler (VEECO NT1100^{6,7}). The optical profiler is adjusted to have the in-plane resolution of 1 μm and the vertical resolution of 0.1 μm, which are the minimum available resolution in this paper. The XYZ stage is designed for large displacement and decoupled motions. When the control to the X stage generates a certain

predictable pattern in the Y stage after enough repetition, this can be regarded as a coupled motion error. Various factors such as fabrication defects, asymmetric design, or thermal energy leaks can have an impact on this coupled motion error.

Three experiments were performed to measure the displacement of the designated motion and the corresponding coupled motion errors for the X stage, the Y stage, and the Z stage separately. The experimental results are plotted in figure 8(a) for the X stage, figure 8(b) for the Y stage and figure 9(a) for the Z stage. In order to verify equation (9), these plots show the trend lines and use V^2 for their X-axes. The trend lines in figures 8(a),

⁷ D MEMS Dynamic MEMS Measurement Option for Wyko NT1100 Optical Profilers www2.veeco.com/pdfs.php/396

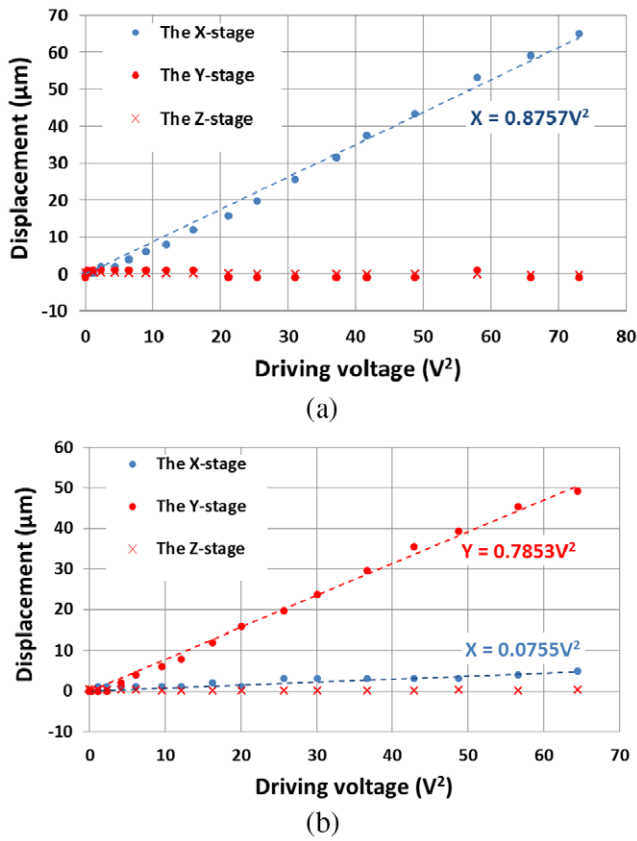


Figure 8. Experimental results of the X stage and the Y stage motion: (a) when the X stage is actuated; (b) when the Y stage is actuated.

(b) shows that the mechanical behaviors of the X stage and the Y stage are proportional to the square of the driving voltage (V^2) as described in equation (9). This indicates that the mathematical analysis in the previous section is valid to predict and control the stage’s motions. There is still a small difference between the trend line and the real experimental data. One main reason for this is material properties used in equation (9); most material properties of silicon are nonlinear and temperature dependent, but equation (9) is based on constant material properties.

Figures 8(a), (b) also indicate that both the X stage and the Y stage are able to generate about $50\mu\text{m}$ for driving voltages of 7.62 and 8.0V, respectively. Between them, the X stage demonstrates more than $60\mu\text{m}$ displacement. These results fit well with the expected behavior from FEA in the previous section. Concerning the coupled motion error, when the X stage or the Y stage is in operation, the Z stage shows random motions with less than $1\mu\text{m}$ amplitude. These motions do not show any pattern and a motion with the amplitude of less than $1\mu\text{m}$ is small enough to be negligible in the XYZ stage, so it is difficult to regard them as coupled motion errors. Based on this observation, the coupled motion errors related to the Z stage can be considered insignificant. However, the X stage shows a repeatable motion pattern when the Y stage is in its operation as shown in figure 8(b). This pattern can be regarded as coupled motion error. The main reason for this coupled motion error is that the temperature rise in the Y stage affects the temperature of the actuator in the X stage and comes from thermal energy leak, not structural coupling. However, the heat generated in

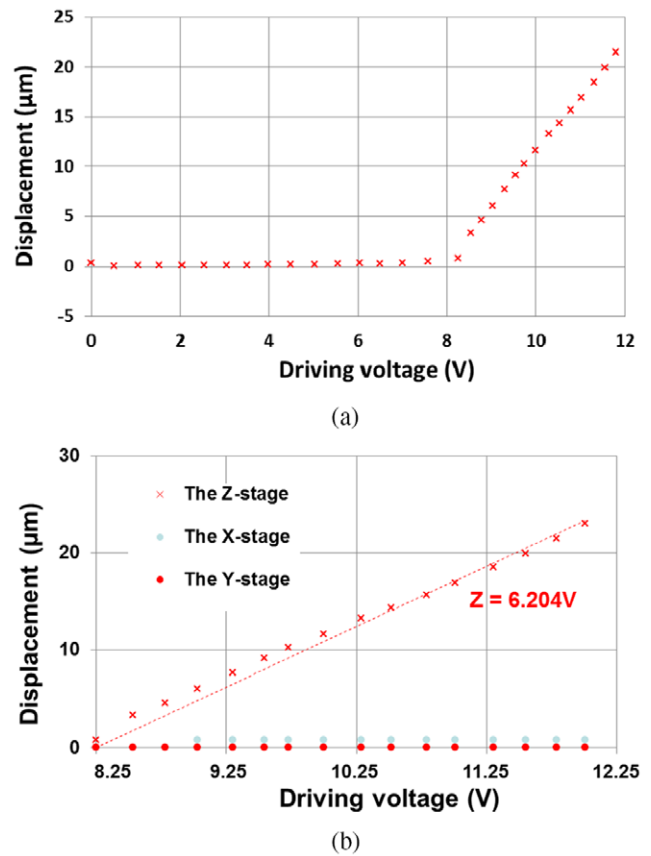


Figure 9. Experimental results of the Z stage displacement in the XYZ stage: (a) when the Z stage is actuated; (b) the post-buckling mode of (a). (The results from actuating the X stage are in blue dots, the results from actuating the Y stage in red dots and the results from actuating the Z stage in red crosses.)

the X stage is well dissipated to the heat sink near the actuator of the X stage, not affecting its coupled motion error substantially. The Z stage is also close to the Y stage, but its coupled motion error is insignificant. This is because the form factor of the Z stage is relatively smaller than the others and the Z stage utilizes a different working principle: buckling. Detailed performance data are presented in table 3.

The displacement of the Z stage is plotted in figure 9(a), which shows different mechanical behaviors from the actuation of the X stage or the actuation of the Y stage. This is because the actuation of the Z stage operates based on the buckling of the beam, not thermal expansion of the bent beams. The pre-buckling mode or bending moment by pure thermal expansion produces the displacement of $1.25\mu\text{m}$ with the driving voltage of 8.25V and the post-buckling mode shows an increment up to $22.91\mu\text{m}$ with the voltage of 12.01V. Since this post-buckling mode will be used in the XYZ stage, this post-buckling mode is plotted separately in figure 9(b) with its trend line and the corresponding coupled motion errors. The slope of the pre-buckling mode is $0.15\mu\text{m V}^{-1}$ and that of the post-buckling mode is $6.76\mu\text{m V}^{-1}$. This big difference indicates not only how the buckling is useful in its stroke, but also when the buckling starts. Over the post-buckling mode, the plastic deformation starts with approximate 12V after several tests, so the Z stage needs to be operated within the driving voltage range between

Table 3. The maximum displacements and the coupled motions of the XYZ stage without compensation.

Target	Actuation Displacement	Coupled motion error without compensation		
		X stage Displacement	Y stage Displacement	Z stage Displacement
The X stage	58.90 μm	–	<0.98 μm	0.32 μm
The Y stage	49.15 μm	4.92 μm	–	0.17 μm
The Z stage	22.91 μm	<0.98 μm	<0.98 μm	–

8.25 and 11.78V to utilize the buckling effect efficiently and assure reliable operations to avoid any plastic deformation.

Detailed values for the maximum displacements and the corresponding coupled motion errors are listed in table 3. The coupled motion error in the X stage by the Y stage is relatively bigger than other factors and needs to be reduced. The compensation algorithm is adapted in the following section in order to reduce these coupled motion error.

4.2. Compensation for reducing coupled motion errors

The coupled motion error of the X stage by the Y stage must be reduced to an acceptable level. As described in equation (7), the displacement of the moving plate is linearly proportional to the square of the driving voltages. This property indicates that the superposition of the actuators rising temperature can be expressed as a summation. The whole response of the XYZ stage can be expressed by the combination of the driving voltages as:

$$\begin{bmatrix} X (\mu\text{m}) \\ Y (\mu\text{m}) \\ Z-1.25 \mu\text{m} \end{bmatrix} = \begin{bmatrix} 0.8757 & 0.0755 & 0 \\ 0 & 0.7853 & 0 \\ 0 & 0 & 6.204 \end{bmatrix} \begin{bmatrix} V_x^2 (V) \\ V_y^2 (V) \\ V-8.25V \end{bmatrix} \quad (9)$$

Based on equation (9), the expected displacement from the XYZ stage can be calculated according to the input voltages. Each term in the matrix in equation (9) is extracted from the slopes of the trend lines in figures 8 and 9. The offset applied to the Z stage is for excluding the pre-buckling mode and utilizing the post-buckling mode only for a straightforward control. One thing to notice is that the matrix in equation (9) is not a diagonal matrix. This means that the coupled motion error is observable at the X stage while the Y stage is in its operation. This coupled motion error can be compensated by controlling the input voltage to the X stage which corresponds to the input voltage to the Y stage. This compensation is described in equation (10) as:

$$\begin{bmatrix} X - X_{\text{off}} (\mu\text{m}) \\ Y (\mu\text{m}) \\ Z-1.25 (\mu\text{m}) \end{bmatrix} = \begin{bmatrix} 0.8757 & 0.0755 & 0 \\ 0 & 0.7853 & 0 \\ 0 & 0 & 6.204 \end{bmatrix} \begin{bmatrix} V_x^2 (V) - V_{\text{off}}^2 (V) \\ V_y^2 (V) \\ V-8.25 (V) \end{bmatrix} \quad (10)$$

where the X_{off} is the x-directional offset and V_{off} is the corresponding input voltage to reduce the coupled motion error. The

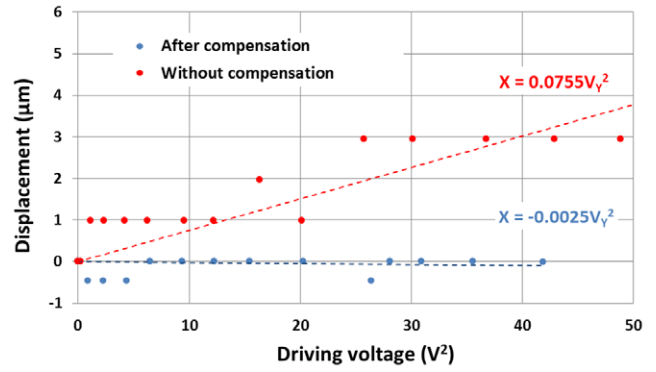


Figure 10. The compensation of the coupled motion error in the X stage by the motion of the Y stage; the red dots are for the original motions and blue dots for the compensated motions.

relationship for V_{off} is $V_{\text{off}} = 0.294V_y$ and its maximum value is 2.75V for the maximum X_{off} of 4.92 μm. Based on these terms, the coupled motion error can be reduced. However, the electrothermal actuators in the XYZ stage are not bi-directional actuators, so it is impossible to actuate the stage in a reverse direction for this compensation. In order to overcome this issue, the offset will be utilized when a backward motion is needed for the compensation operation. Due to the offsets, the maximum displacement of the X stage will be reduced to 53.98 μm from 58.90 μm.

The matrix in equation (9) can be expressed as its inverse form as equation (10). The appropriate input voltages can be calculated for the desired position information based on equation (10).

$$\begin{bmatrix} V_x^2 - V_{\text{off}}^2 (V) \\ V_y^2 (V) \\ V-8.25 (V) \end{bmatrix} = \begin{bmatrix} 1.1419 & -0.1098 & 0 \\ 0 & 1.2734 & 0 \\ 0 & 0 & 0.1612 \end{bmatrix} \begin{bmatrix} X - X_{\text{off}} (\mu\text{m}) \\ Y (\mu\text{m}) \\ Z-1.25 (\mu\text{m}) \end{bmatrix} \quad (11)$$

Figure 10 compares the original experimental data with this compensation based on equation (11). With this compensation, the X stage remains at its designated position with less than 1 μm variation while the Y stage generates motions up to 49.15 μm.

4.3. The frequency response of the proposed XYZ stage

The frequency responses of the XYZ stage are measured separately for in-plane motions and out-of-plane motions. For the X stage and the Y stage, an Agilent⁶ fast-fourier-transform (FFT) analyzer with the frequency response measurement method [31] is used. With this experimental set-up, the first resonance frequency of the X stage is observed near 0.51 kHz and the Y stage is 1.06 kHz. These values are similar to those in their original XY stage [16] as expected. In addition, the first frequency of the X stage is half of that of the Y stage. This comes from the design difference between the X stage and the Y stage; the X stage supports both the Y stage and the Z stage,

Table 4. MEMS-based positioning stages in specific cases.

Reference	Range of motion (μm)		1st mode resonant frequency (Hz)		Stiffness (N m^{-1})	Force (mN)	Actuation mechanism and applications
	X	Y	X	Y			
Lantz <i>et al</i> 2007 [32]	± 60	± 60	185	210	90.5	~ 10	Electromagnetic actuator Probe-storage
Fowler <i>et al</i> 2012 [33]	16	15	816	820	–	–	Electrostatic actuator AFM scanning
Duc <i>et al</i> 2008 [34]	17	11	–	–	74	0.814	Polymer actuator Micro-gripper
This study	53.98	49.15	510	1060	900	~ 4.5	Electrothermal actuator

but the Y stage holds the Z stage only. This difference from the nested structure results in different mass which is not unusual in a serial kinematic mechanism (SKM). In order to overcome this property, the stiffness of the X stage and the Y stage need to be re-designed. The stiffness can be calculated analytically from equation (3) and equation (4). Another approach to overcome this limit is to utilize the parallel kinematic mechanism (PKM), where two identical X stages which are perpendicular to each other are connected for the in-plane motions⁴ [5]. However, PKM makes its output tightly coupled, which needs a non-linear mathematical model to obtain its relationships between the input voltages and the output displacements. This requires considerable design effort to build the mathematical model and preprocessing time before each operation.

For the Z stage, a Polytec MSA-500 Micro System Analyzer^{6,8} is adapted for out-of-plane responses. With this equipment, the first frequency response of the Z stage is observed at 78.7 kHz. This value is very close to a single Z stage [19], because the Z stage used in the XYZ stage does not have significant difference from the adapted design.

Based on the observation on the frequency responses, the presented XYZ stage is appropriate for the operations with the speed of less than 100 Hz and forces larger than a few mN level. These specifications indicate that the presented stages are desirable at micro-manipulation for micro-assembly or cell-manipulation.

4.4. The characteristics of the proposed XYZ stage

The range of motion and the frequency response of the presented stage are analyzed in the previous section. The presented stage demonstrates relatively larger strokes, especially for the Z-motion than the stages in table 1. This indicates the usability of the nested structure design to merge the three independent stages into one without significant interference. In addition to this, no special fabrication methods are needed. This is because an appropriate Z stage can be chosen without design constraints or fabrication limitations from the other engaged stages in the nested structure design.

Based on these features, the presented stage in this study can be regarded as a good candidate for the environment requiring a displacement larger than $50 \mu\text{m}$, a force larger than

1 mN, a stiffness of more than 100 N m^{-1} , a driving voltage of less than 20 V, and a reliable operation at low frequency less than 500 Hz. As listed in table 4, the nano-positioner designed for probe-storage applications should generate large strokes and be stable against any external disturbance [32]. The nano-positioner designed for AFM applications has to operate at high frequency [33]. The micro-gripper needs to be stiff and able to generate enough displacement at low frequency [34]. Based on these features, micro-manipulation or micro-assembly can be reasonable applications for the presented stage, which does not require high speed operation, but large force and displacement. Two two-DOF motion stages with probes are reported to grip and rotate a particle of $14.8 \mu\text{m}$ diameter successfully [16]. These operations can be extended with the presented XYZ stage for more delicate operations. The cooperation of three two-DOF stages are reported for six-DOF motions in MEMS [35], which also can be implemented by two XYZ stages presented in this study.

5. Conclusions

In this paper, we have demonstrated design, fabrication, and testing of the MEMS based XYZ stage. The presented XYZ stage is designed and built by merging three individual stages through the nested structure. With this approach, three-DOF motions are obtained with tens of microns of strokes. This implementation shows that utilizing existing MEMS actuators, instead of developing totally new designs, can be one way to develop a device with various advantages, such as reduction in the design process time and expected risks.

For successful implementation of the XYZ stage, several additional features were required and incorporated: (a) the embedded electric connection to control the Y stage and the Z stage inside the X stage reliably; (b) the electric isolation among three stages to prevent any motion error by leaking electrical currents; (c) the floating frames to hold the embedded Y and Z stages in their positions for accurate motions; and (d) the floating blocks to hold the electrothermal actuators in their positions for efficient operations. With these features, the presented XYZ stage demonstrates successfully the range of motion of $53.98 \times 49.15 \times 22.91 \mu\text{m}$ along X, Y, and Z axes respectively. During this demonstration, the coupled motion error is observed but can be reduced to less than 1% with the presented compensating algorithm.

⁸ Polytec MSA-500 Micro System Analyzer www.polytec.com/us/products/vibration-sensors/microscope-based-systems

The nested structures for the XYZ stage prove its usefulness to achieve design goals with low cost and high reliability by merging already existing MEMS systems. When their fabrication methods are compatible with others, other various MEMS devices are possible; instead of the Z stage, a micro-gripper can be embedded onto the motion platform of the Y stage. This approach can provide a pick-move-and-release operation through the combination of the XY stage and the micro-gripper without significant design process and effort.

Acknowledgments

The authors would like to thank Dr Richard Gates for his valuable advice and support on the experiments for the frequency response. This research was performed in part in the NIST Center for Nanoscale Science and Technology Nano Fabrication Clean Room. This work was supported by the Measurement Science for Intelligent Manufacturing Robotics and Automation Program of the Intelligent Systems Division, Engineering Laboratory, National Institute of Standards and Technology, USA.

References

- [1] Donald B R, Levey C H and Paprotny I 2008 *J. Microelectromech. Syst.* **17** 789–808
- [2] Beyeler F, Neild A, Oberti S, Bell D J, Sun Y, Dual J and Nelson B J 2007 *J. Microelectromech. Syst.* **16** 7–15
- [3] Choi Y-M, Gorman J J, Dagalakis N G, Yang S H, Kim Y and Yoo J M 2012 *J. Micromech. Microeng.* **22** 105012
- [4] Greminger M A, Sezen A S and Nelson B J 2005 A four degree of freedom MEMS microgripper with novel bi-directional thermal actuators *Proc. IROS 2005: IEEE/RSJ Int. Conf. on Intelligent Robots and Systems (Aug. 2005)* pp 2814–9
- [5] Yao Q, Dong J and Ferreira P M 2007 *Int. J. Mach. Tool Manu.* **47** 946–61
- [6] Sun L, Wang J, Rong W, Li X and Bao H 2008 *J. Micromech. Microeng.* **18** 125004
- [7] Mukhopadhyay D, Dong J, Pengwang E and Ferreira P 2008 *Sensors Actuators A* **147** 340–51
- [8] Ando Y 2004 *Sensors Actuators A* **114** 285–91
- [9] Liu X, Kim K and Sun Y 2007 *J. Micromech. Microeng.* **17** 1796–802
- [10] Takahashi K, Mita M, Fujita H and Toshiyoshi H 2007 Topological layer switch technique for monolithically integrated electrostatic XYZ stage *MEMS 2007: IEEE 20th Int. Conf. On MEMS (Hyogo, Jan. 2007)* pp 651–4
- [11] Johnes R M 2008 *Buckling of Bars, Plates, and Shells* (Blacksburg, VA: Bull Ridge Publishing) pp 73–5
- [12] Chen W C, Chu C C, Hsieh J and Fang W 2003 *Sensors Actuators A* **103** 48–58
- [13] Aioubi M Y A, Djakov V, Huq S E and Prewett P D 2004 *Microelectron. Eng.* **73/74** 898–903
- [14] Bergna S, Gorman J J and Dagalakis N G 2005 Design and modeling of thermally actuated MEMS nanpositioner *Proc. of IMECE 2005: 2005 ASME Int. Mech. Eng. Cong. and Expo. (Orlando, FL)*
- [15] Kim Y S, Dagalakis N G and Gupta S K 2011 A two degree of freedom nanopositioner with electrothermal actuator for decoupled motion *Proc. IDETC/DTM 2011, ASME (Washington, DC, Aug. 2011)*
- [16] Kim Y S, Yoo J M, Yang S H, Nicholas N G and Gupta S K 2012 *J. Micromech. Microeng.* **22** 085029
- [17] Miller K, Cowen A, Hames G and Hardy B *SOIMUMPs Design Handbook Revision 4.0* (www.memscap.com/mumps/documents/SOIMUMPs.dr.v4.pdf)
- [18] Kim Y S, Nicholas N G and Gupta S K 2012 Design, fabrication and characterization of a single-layer out-of-plane electrothermal actuator for SOI-MEMS applications *Proc. 2012 Performance Metrics for Intelligent Systems Workshop (College Park, MD, Mar. 2012)*
- [19] Kim Y S, Dagalakis N G and Gupta S K 2013 *J. Micromech. Microeng.* **23** 055008
- [20] Kim Y S, Dagalakis N G and Gupta S K 2012 Design and Fabrication of a Three-DoF MEMS Stage Based on Nested Structures *Proc. ASME 2012 International Conference IDETC/CIE 2012 (Chicago, IL, Aug. 2012)*
- [21] Zhu Y, Corigliano A and Espinosa H D 2006 *J. Micromech. Microeng.* **16** 242–53
- [22] Paros J M and Weisbord L 1965 *Mach. Des.* **37** 151–6
- [23] Luo J L, Flewitt A J, Spearing S M, Fleck N A and Milne W L 2005 *J. Micromech. Microeng.* **15** 1527–35
- [24] Que L, Park J S and Gianchandani Y B 2001 *J. Microelectromech. Syst.* **10** 247–54
- [25] Baker M S, Plass R A, Headley T J and Walraven J A 2004 *Final Report: Compliant Thermomechanical MEMS Actuators LDRD* www.memscap.com/tech-info/doc/thermal_actuator_SAND.pdf
- [26] Kim J, Choo H, Lin L and Muller R S 2006 *J. Microelectromech. Syst.* **15** 553–62
- [27] Gallagher C J 1952 *Phys. Rev.* **88** 721–2
- [28] Beer F P and Johnston E R Jr 1992 *Mechanics of Materials* 2nd edn (New York: McGraw-Hill) pp 650–1
- [29] Cerda E and Mahadevan L 2003 *Phys. Rev. Lett.* **90** 074302
- [30] Ebefors T, Mattsson J U, Kälvesten E and Stemme G 1999 A walking silicon micro-robot *Proc. 10th Int. Conf. on Solid-State Sensors and Actuators Transducers '99*
- [31] Gorman J J, Kim Y S and Dagalakis N G 2006 Control of MEMS nanopositioners with nano-scale resolution *ASME Proc. ASME Int. Mechanical Engineering Conf. and Exh. (Chicago, USA)*
- [32] Lantz M A, Rothuizen H E, Drechsler U, Häberle W and Despont M 2007 *J. Microelectromech. Syst.* **16** 130–9
- [33] Fowler A G, Laskovski A N, Hammond A C and Moheimani S O R 2012 *J. Microelectromech. Syst.* **21** 771–3
- [34] Duc T C, Lau G-K and Sarro P M 2008 *J. Microelectromech. Syst.* **17** 823–31
- [35] Yang S H, Kim Y S, Yoo J M and Dagalakis N G 2012 *Appl. Phys. Lett.* **101** 061909